Mechanics of Advanced Composite Structures 9 (2022) 163 – 171

Semnan University

Mechanics of Advanced Composite Structures

journal homepage: http://MACS.journals.semnan.ac.ir

Green Anticorrosion Coating with Low VOCs Emission using Moringa Oleifera Leaves Extract

W.M.K.W.M. Ikhmal [a], S.M. Syaizwadi [a], N.M.N. Amirah [a], W.A.W. Rafizah [b], W.N.W.M. Norsani [b], M.G.M. Sabri [a,*]

[a] *Advanced Nano Materials (ANoMa) Research Group, Faculty of Science and Marine Environment, University Malaysia Terengganu, 21030 Kuala Nerus, Terengganu, Malaysia*

[b] *Faculty of Ocean Engineering Technology and Informatics, University Malaysia Terengganu, 21030 Kuala Nerus, Terengganu, Malaysia*

KEYWORDS

Paint coatings;
Plant extract;
Marine;
Volatile organic compounds.

ABSTRACT

Air pollution is an increasing prevalence of environmental diseases. Previously, hazardous air pollutants (HAPs) on the ozone layer, which primarily constitute volatile organic compounds (VOCs), have become a major public concern. As a result, the Environmental Protection Agency (EPA) has introduced a strict regulation on the limit of VOCs content for various daily products such as paints and solvents to reduce the risk. Hence, the study aims to develop an eco-friendly coating with low VOCs content per the imposed regulation by deploying the leaves extract of *Moringa Oleifera* (MOE) for marine vessel protection. The formulated coating was characterized by using optical, electrochemical, and morphological analysis to study the effectiveness of its barrier property against the aggressive solution of seawater. Additionally, measurement of its VOCs content was conducted following the ASTM D2369-03. The results obtained suggested that the incorporation of 1 wt.% of MOE of C2 increased the resistivity of coating in reducing the penetration of ionic electrolytes up to 91.2% while exhibiting the traits of low VOCs content category at a value of 198 g/L.

1. Introduction

The age of modernization with rapid progress in technology has induced various detrimental impacts on human health and the environment. As the population increased, the need to sustain a comfortable daily life by exploring the resources on land and water has generated a massive amount of waste and pollution. One of the most critical issues of air pollution is the release of volatile organic compounds (VOCs) into the atmosphere. In general, VOCs are defined as organic chemical compounds that can evaporate at ambient temperature and pressure. It is a widespread atmospheric species produced by vehicle emission, combustion in factories, and various available products on the market, such as paint [1,2]. The VOCs posed adverse effects due to their ability to form the harmful photochemical ozone smog with inherent characteristics of being carcinogenic and mutagenic [3]. Examples of major VOCs substances include benzene, toluene, ethylbenzene, and xylene (BTEX). When a human is exposed to VOCs daily either due to its emission at indoor or outdoor, symptoms, as follows, can occur; (1) headache, (2) fatigue, (3) dizziness, (4) nausea, (5) nose, throat, and eye irritation and (6) visual disorders [4]. The result of VOCs exposure in the long term includes severe health problems such as leukemia, neural tube defects in the baby, and damage to the lungs and nervous system [5].

The study focuses on the coating's emission of VOCs during the application and curing processes when applied to a marine vessel. The notion is that the procedure is considered a major anthropogenic source of VOCs for the aquatic environment [6]. The deployment of coating in protecting the marine vessel and construction is common. This requirement is because of the nature of seawater that can corrode metallic structures leading to the failure of a system [7]. Thus, to reduce the cost of repairing and

* Corresponding author. Tel.: +609-6683760
E-mail address: mohdsabri@umt.edu.my

DOI: 0.22075/macs.2022.22771.1328
Received 2021-02-25; Received in revised form 2022-01-22; Accepted 2022-02-21.

maintenance, an effective coating is a must. When a coating begins to cure and starts to release VOCs, the substance will travel to the atmosphere. Over time, the accumulated VOCs in the atmosphere will react with other chemicals, including nitrogen oxides and sulfur, released from industrial activities. The chemical interaction catalyzed by the sunlight can produce ground-level ozone (O3) that is slowly increased in concentration as more VOCs are converted. When the concentration reaches a certain level, it will fall on humans, animals, and plants via dry or wet deposition routes. These substances usually act as a type of oxidant that may initiate various negative impacts. For example, O_3 can induce oxidative stress on us, causing an imbalance in the amount of both free radicals and antioxidants yielding in cell and tissue damage [8]. Other than that, if the protective layer of plants and animals is unable to stop these oxidants from passing into its intracellular surface, severe inflammatory and failure of reparative response with proteins and lipids damage may occur [9,10]. Hence, concerns about reducing the VOCs emission through incorporating natural resources in this new formulation have become a critical aspect of this project.

In summary, the coating is developed by using secure natural products of the ecosystem to ensure minimal environmental effects. The formulation includes a new type of additive from the leaves of Moringa Oleifera, which are believed to enhance the general strength of the coating and have a contribution in reducing the amount of solvent being used. The plant is selected because various studies have highlighted its capability as an antioxidant and antimicrobial [11-13], the two primary properties to reduce the corrosion rate in the marine environment. Moreover, the plant is abundant and easily available since many considered it as a byproduct with no practical application. Besides, incorporating plant extract as an additive in coating proved to be an exciting field to explore as the previous research displayed excellent outputs with the incorporation of Leucaena leucocephala [14], Andrographis Paniculata [15], and henna leaves [16]. As the primary sources of VOCs in coating formulation are based on the amount and type of solvent, the decrease of solvent in this formulation while ensuring the overall strength remains the same could potentially highlight the capability of the plant extract in various future applications.

2. Materials and Methods

2.1. Materials

The stainless-steel grade 316L (SS316L) with the corresponded composition in Table 1 [17] was prepared following ASTM E3-11, where each was cut into a rectangular shape with a dimension of 25 mm x 25 mm x 3 mm. The steel from each specimen was polished with emery paper of various grades (240, 600, 800, and 1000) using Presi Mecapol model P255 U (PRESI, Shah Alam, Malaysia). The polishing process was performed to achieve a mirror-like surface. The polished specimens were rinsed with acetone and distilled water and immediately dried using a clean tissue to store in a dry box before use. The dried powder of Moringa Oleifera was bought from Secret Barn Sdn Bhd and other chemicals such as methyl isobutyl ketone (MIBK), calcium carbonate ($CaCO_3$), and zinc oxide (ZnO) were purchased from Chembio Technology Sdn. Bhd. Water-white (WW) rosin was supplied by Urich Technology. All the chemicals were used with no further purification to avoid uncontrolled chemical reactions.

2.2. Crude extract preparation

The dry powder of *Moringa Oleifera* was soaked in 80% ethanol following the ratio of 1:10. The mixture was placed in the conical flask and sealed using aluminum foil before being left on a shaker for 24 hours. The soaking process was used to separate the active compounds within the powder from its solid part. Then, the mixture was filtered through the Whatman no. 1 filter paper (Sigma-Aldrich, Petaling Jaya, Malaysia) and evaporated using the rotary evaporator to obtain the crude extract. The collected crude extract was stored in the refrigerator (4 °C) before use to ensure its freshness and avoid bacterial contamination.

2.3. Coatings formulation and application

The coating formulation presented in Table 2 was modified by using *Moringa Oleifera* crude extract as an additive. The WW rosin act as the binder by providing the overall resistance to the coating system and methyl isobutyl ketone (MIBK) as the solvent. ZnO and $CaCO_3$ were used as the pigment to enhance the structure of the coating. The coating preparation was started by mixing the WW rosin and MIBK for 4 hours on a stirrer to ensure the mixture is well dispersed. Then, the pigments were then added slowly into the mixture with continuous stirring until no coagulant was present. Finally, the crude extract was inserted and stirred for 2 hours until it dispersed into the coating. The coating is applied on the surface of SS316L using a brush with a standard thickness of 90 μm. The coated specimens were dried in an oven at a temperature of 52 ℃ for 24 hours. After drying, the samples were stored in a desiccator before proceeding with sample testing.

Table 1. Chemical composition of stainless steel 316L (SS316L) [17]

Element	C	Mn	P	S	Si	Cr	Ni	Mo	N	Fe
%	0.03 max	2.00 max	0.045 max	0.03 max	0.75 max	16.00 – 18.00	10.00 – 14.00	2.00 – 3.00	0.10 max	Balance

Table 2. Formulation of coatings by wt.%

Component/Paint	C1	C2	C3	C4
WW Rosin	60	60	60	60
MIBK*	10	10	10	10
$CaCO_3$	10	10	10	10
ZnO	20	19	17	15
MOE*	0	1	3	5

*MOE: Moringa Oleifera leaves extract
*MIBK: Methyl isobutyl ketone

2.4. Fourier Transform Infrared (FTIR) Spectroscopy

The presence of functional groups within the crude extract and coatings were identified by using FTIR. The crude extract was examined by penetrating a beam of infrared into the sample and measuring the difference in output transmittance path. The characterization was conducted using a Thermo Nicolet 380 FTIR spectrometer model (Thermo Fisher Scientific, Waltham, Ma, USA) at the frequency range from 400 cm^{-1} to 4000 cm^{-1}.

2.5. Total VOCs content Analysis

The VOCs content was analyzed on the coating with the best performance. The coating formulation was reformulated to follow the ASTM D2369-03, a standard test method for the volatile content of coatings by using only 3 mL of solvent [18]. An aluminum foil formed into disc shapes with a diameter of 58 mm and 18 mm in height. The weight of the aluminum disc (W_1) was measured using a digital analytical balance and placed in an oven at 110 ± 5 ℃ for 30 minutes. The coating mixture was added slowly to the aluminum disc, which contained 3 mL of solvent. The coating mixture was stirred gently with a paper clip, and the aluminum disc with coating was next weighed as W_2. The specimens were then dried inside an oven at 110 ± 5 ℃ for 60 minutes, and then the samples were taken out for weight loss measurement (W_3). The weight fraction of the volatile component (Wv) was calculated based on Equation 1, where W_1 is the weight of aluminum disc with coating before heating, W_2 is the weight of aluminum disc with coating after heating, and W_3 is the weight of the coating. The weight fraction of solid (W_s) was then determined by using Equation 2.

$$W_V = \frac{W_1 - W_2}{W_3} \quad (1)$$

$$W_S = 1 - W_V \quad (2)$$

2.6. Immersion Test

The immersion test was conducted using artificial seawater in a laboratory to investigate the resistance properties of coated and uncoated SS316L. The specimens were immersed in a container that contains a specific amount of artificial seawater, calculated according to ASTM G31-72. Coated and uncoated SS316L were then hung inside the container, where it was tied to the casing of the container. Specimens were collected every 3 days for corrosion and surface characteristics such as Electrochemical Impedance Spectroscopy (EIS), potentiodynamic polarization (PP), and Scanning electron microscope (SEM).

2.7. Electrochemical Impedance Spectroscopy (EIS)

The impedance and capacitance of the coating system to the aggressive solution of various corrosive agents of seawater were measured using EIS. The analysis probed the effect of corrosion on metal and determined the amount of electrolytes penetration into the surface of the coating. The evaluation was employed using alternating current (AC) with an Autolab PGSTAT302N (Metrohm, Herisau, Switzerland) connected to the NOVA software 1.10 to analyze and fit the data obtained. The study also uses the three-electrode cells, which include the reference electrode (RE) for measuring the potential of the working electrode (WE), as the studied sample, and a counter electrode (CE) made of platinum for allowing the current to pass through. The impedance measurement was examined within the frequency range from 10 MHz to 100 kHz at the amplitude of 10 mV (RMS).

2.8. Potentiodynamic Polarization (PP)

The resistance of the sample toward the corrosion was inspected using PP, which supplies the current and voltage to measure the inhibitive mechanism in regards to the properties of the medium. The changes in the potentiodynamic current potential curves were recorded within the potential range from -1.0 V to 0.3 V with 10 mVs^{-1} of scanning rate. In addition, the density (8.03 g/cm^3), the surface area (6.25 cm^2), and the equivalent weight (25.65 g/mol) were used as a reference parameter to ensure that the reading is accurate during the measurement process. Finally, the data was analyzed and fitted by using NOVA software 1.10.

2.9. Scanning Electron Microscope (SEM)

In this study, the surface morphology of the coated samples was examined using a JEOL JSM-6360LA SEM (JEOL USA, Peabody, USA). SEM analyzed the coated samples to correlate the microstructural results with the data obtained from EIS and PP. The observation was conducted at the magnification of x1000 with an accelerating voltage of 15kV.

3. Results and Discussion

3.1. Fourier Transform Infrared Spectroscopy (FTIR)

The study of FTIR is to investigate the presence of the functional group in the MOE and within the formulated coatings, as shown in Figure 1 and Figure 3, respectively.

The corresponded characteristics were tabulated in Table 3 The discussion and selection of the result obtained were based on the structure of major compounds in the leaves: myricetin and gallic acid, as displayed in Figure 2 [19].

In total, there are four wavenumbers detected that correspond to the structures illustrated in Figure 3. First, at the wavenumber 3315.63 cm^{-1}, a strong and broad appearance of carboxylic acids was identified. Then, at peak 1570.06 cm^{-1}, the functional group of carbonyl was detected with a strong appearance. Additionally, an alkene group was presented with a medium appearance at wavenumber 1402.25 cm^{-1}. Lastly, the primary alcohol group with a strong appearance was observed at 1031.92 cm^{-1}. Thus, the identified functional groups served as a preliminary assessment to prove the presence of the mentioned compounds.

Moreover, these functional groups can also be discerned to possess multiple heteroatoms, essential components which may give the coating higher resistance toward free ions penetration and increase adhesive property [20].

Figure 3 shows the IR spectra for coatings with different wt.% of MOE where the discussion was based on the two highlighted regions. Based on region 1, which is in the range of 3100 cm-^{1}-3605 cm^{-1}, changes in the carboxylic acid concentration were observable. As the incorporation of MOE increased, coatings unexpectedly exhibit a lower concentration of the targeted functional group.

The obtained result is possibly due to the dissociated process as each of the coating components begins to combine. As for region 2 in the range of 900 cm^{-1}-1120 cm^{-1}, the addition of MOE results in a new presence of a peak that may be corresponded to the primary alcohol, as depicted in Table 3.

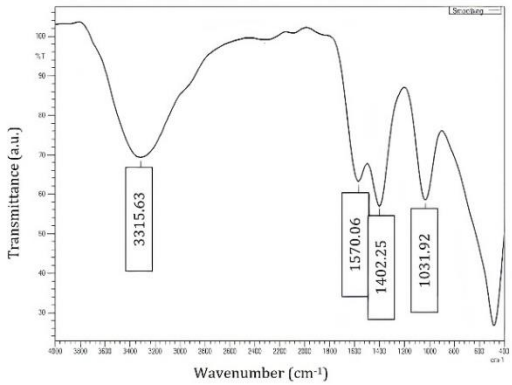

Fig. 1. FTIR spectrum of *Moringa Oleifera* extract (MOE)

Table 3. Peak characteristic of Moringa Oleifera extract (MOE)

Wavenumber (cm^{-1})	Bond	Functional group	Appearance
3315.63	R-COOH	Carboxylic acid	Strong & broad
1570.06	C=O	carbonyl	Strong
1402.25	C=C	Alkene	Medium
1031.92	O-H	Primary alcohol	Strong

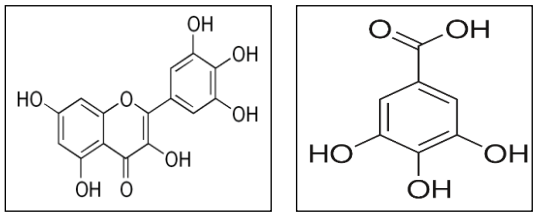

(a) (b)

Fig. 2. Molecular structures of the major compounds of MOE (a) myricetin and (b) gallic acid [19]

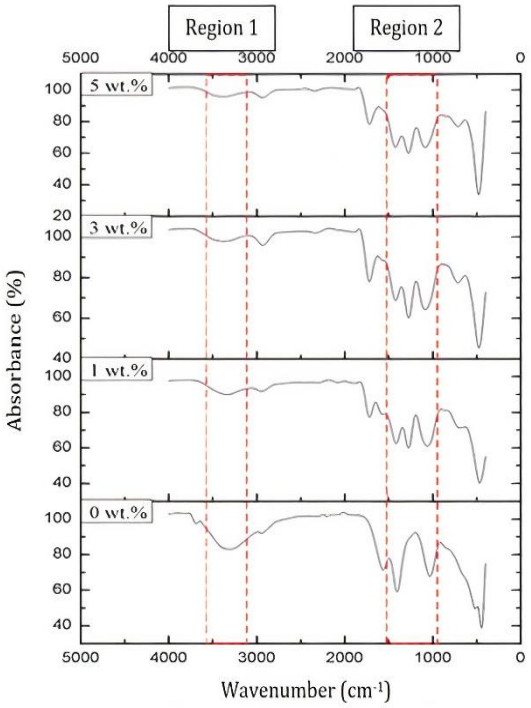

Fig. 3. FTIR spectra of coatings with and without MOE

3.2. Electrochemical Impedance Spectroscopy (EIS)

The electrochemical analysis was used to analyze the barrier behavior of coating ranging from its outermost surface to the coating/metal interface. The characterization was conducted for the coated and uncoated samples immersed for 3-15 days in seawater at room temperature. An electrical equivalent circuit containing two resistors and two capacitors connected in parallel is employed to mimic the behavior of the degradation process that occurred on a coating when exposed to a corrosive medium [21]. By using the method, parameters including the coating resistance (R_c), coating capacitance (C_c), charge transfer resistance (R_{ct}), and double-layer capacitance (C_{dl}) are obtained and tabulated in Tables 4, 5, 6, and 7, respectively. From table 4, the incorporation of MOE as an additive in the coating yielded a sharp increase in the R_c values and began to fall after the added concentration exceeds 1 wt.%. The maximum R_c obtained by C2 from the analysis marks the optimum coating performance during its initial exposure to the aggressive solution. With the increase of the R_c, the capability of the coating outer layer in blocking the penetration of ions and reducing the formation of pores also increases significantly. As for the decrease in the R_c for C3 and C4, the phenomena can be attributed to the lower rate of additive dispersion in the coating matrix, causing the overall matrix system to decline and become more amorphous. The amorphous state of the coating is expected to boost the ionic mobility to pass through the coating forming multiple pores and cracks until it breached into the deepest layer at the coating/metal interface [22]. During the immersion period from 3-9 days, the R_c values for C2 decreased due to the penetration of electrolytes. However, as coatings begin to saturate, the physical interaction begins to stabilize and forms a tougher layer, as shown during 12-15.

Table 5 shows the parameters of C_c that represent the amount of water being accumulated inside the coating. During the 15 days of immersion, C1, C3, and C4 displayed a general increase in the C_c values denoting the constant increase in the rate of electrolyte absorption by the coating layer. However, it is interesting to point out that all coatings have a relatively similar C_c with their previous measurement up till the 12th day which signifies a lower effect of water due to the insignificant overall amount being absorbed. The drastic changes in C1, C2, and C3 were observed on the 15th day, where the water absorbed at this point has caused the coating structure to become saturated. As for C2, although the coating has an increase in C_c values, the changes are not as abrupt as in the other samples, indicating a more stable barrier. The R_{ct} parameter, as tabulated in Table 6 is crucial to assessing the susceptibility of the protected specimen to corrosion. Commonly, it is used with the C_{dl} measurement as displayed in Table 7 to understand the passive ability of coating in preventing corrosion from being initiated on the metal surface. Based on Table 6, at the initial immersion stage, C2 showed a superior barrier property compared to other coatings by having the highest R_{ct} values of 14600 Ω with a low C_{dl} value of 0.08 μF. From 3-6 days of immersion, C1, C2, and C3 showed a similar trend of decreasing R_{ct} which agrees with the finding of R_c. Nevertheless, the values began to increase in general for C1, C2, and C3 from day 9th to 15th. The decrease during the initial stage is attributed to the same phenomena of R_c where the coating has started to be penetrated by aggressive ions inducing a lower barrier defense. But, as the coating begins to stabilize, the increase in the R_{ct} values can be observed in the later stage. From the analysis of R_{ct}, coating with 1 wt.% of MOE (C2) displayed an optimum performance with a higher R_{ct} parameter throughout the immersion test. As for the C_{dl} parameters in Table 7, coatings with MOE concentration up to 3 wt.% displayed a similar measurement even till the last day of immersion. The state of low and comparable C_{dl} values means that the formation of the delaminated area underneath the coating is none or insignificant. These findings suggest that the immersion period of 15 days has only affected the upper part structure of the coating, and its lowest part at the metal/coating interface has not been majorly disturbed. Nevertheless, the measurement which displayed a slight increase in the C_{dl} amount gives a good prediction of the coating behavior if the immersion period is prolonged.

3.3. Potentiodynamic Polarization

The study of potentiodynamic polarization analyzes the behavior of coatings' inhibitive ability towards corrosion via anodic and cathodic mechanisms. The measurements of the coated and uncoated samples on the 15th day were recorded in Table 8 and Figure 4. The incorporation of MOE increases the resistance of coating (C2) by moving the value of corrosion potential, E_{corr} towards the noble region, which was from -0.36346 V to -0.29144 V relative to the bare steel [23, 24]. The other formulated coatings showed a shift towards the negative region. However, in general, the measured samples still retain a more noble position than the bare metal, except for C4 with the highest MOE concentration. A more electropositive value signifies higher passivation or blocking ability while the higher electronegative values describe vice versa.

Table 4. Coating resistance (R_c) values during the immersion period of 15 days

Day	Coating resistance, R_c (Ω)				
	Bare	**C1**	**C2**	**C3**	**C4**
3	-	3.64 x10^3	96.60 x10^3	3.39 x10^3	46.00 x10^3
6	-	2.29 x10^3	32.80 x10^3	2.85 x10^3	8.75 x10^3
9	-	10.8 x10^3	2.42 x10^3	1.80 x10^3	3.11 x10^3
12	-	3.91 x10^3	5.01 x10^3	0.24 x10^3	2.10 x10^3
15	-	6.07 x10^3	6.29 x10^3	2.80 x10^3	0.32 x10^3

Table 5. Coating capacitance (C_c) values during the immersion period of 15 days

Day	Coating capacitance, C_c (F)				
	Bare	**C1**	**C2**	**C3**	**C4**
3	-	4.05 x10^{-9}	10.30 x10^{-9}	36.80 x10^{-9}	85.90 x10^{-13}
6	-	13.00 x10^{-9}	9.00 x10^{-13}	14.10 x10^{-9}	3.19 x10^{-9}
9	-	17.50 x10^{-9}	3.83 x10^{-9}	121.00 x10^{-9}	15.90 x10^{-9}
12	-	5.16 x10^{-9}	26.40 x10^{-9}	247.00 x10^{-9}	30.20 x10^{-9}
15	-	530.00 x10^{-6}	77.20 x10^{-9}	0.60 x10^{-6}	1.87 x10^{-6}

Table 6. Charge transfer resistance (R_{ct}) values during the immersion period of 15 days

Day	Charge transfer resistance, R_{ct} (Ω)				
	Bare	**C1**	**C2**	**C3**	**C4**
3	6.08 x10^3	12.18 x10^3	14.60 x10^3	8.25 x10^3	32.3 x10^3
6	17.7 x10^3	1.30 x10^3	1.59 x10^3	1.62 x10^3	11.00 x10^3
9	0.40 x10^3	4.15 x10^3	3.97 x10^3	2.35 x10^3	3.01 x10^3
12	0.02 x10^3	6.45 x10^3	2.76 x10^3	0.47 x10^3	3.95 x10^3
15	0.43 x10^3	9.91 x10^3	12.32 x10^3	5.92 x10^3	0.58 x10^3

Table 7. Double-layer capacitance (C_{dl}) values during the immersion period of 15 days

Day	Double-layer capacitance, C_{dl} (F)				
	Bare	**C1**	**C2**	**C3**	**C4**
3	33.10 x10^{-6}	0.020 x10^{-6}	0.08 x10^{-6}	0.25 x10^{-6}	0.02 x10^{-6}
6	25.80 x10^{-6}	0.30 x10^{-6}	0.07 x10^{-7}	1.03 x10^{-6}	0.12 x10^{-6}
9	17.40 x10^{-6}	3.17 x10^{-6}	0.37 x10^{-6}	1.42 x10^{-6}	0.41 x10^{-6}
12	2.52 x10^{-6}	0.40 x10^{-6}	0.46 x10^{-6}	10.8 x10^{-6}	1.04 x10^{-6}
15	11.70 x10^{-6}	3.78 x10^{-6}	0.84 x10^{-6}	2.94 x10^{-6}	18.40 x10^{-6}

Table 8. Polarization measurement of samples after 15 days of immersion

Sample	E_{corr} (V)	i_{corr} (A/cm2)	Corrosion rate (mm/year)	Polarization resistance (Ω)	Inhibition efficiency, η (%)
Bare	-0.363	2.54 x10^{-5}	0.26	4886	
C1	-0.349	6.91 x10^{-7}	7.22 x10^{-3}	35018	86.0
C2	-0.291	4.44 x10^{-7}	4.64 x10^{-3}	55083	91.2
C3	-0.336	3.12 x10^{-6}	32.62 x10^{-3}	23587	79.3
C4	-0.409	1.96 x10^{-5}	0.21	3852	26.8

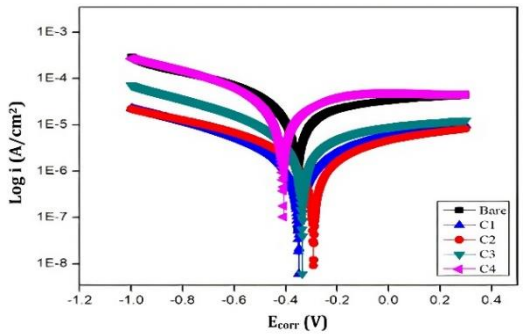

Fig. 4. Tafel plots for samples after 15 days of immersion

The measurement of corrosion current density, i_{corr} can also be used to indicate the overall rate of corrosion. For example, when there is a decrease in this value, the sample is said to have better corrosion resistance or blocking action. Additionally, the decrease of i_{corr} may also indicate that the sample exhibits a mixed type of inhibitive action towards the corrosion process. It is a passivation mechanism where the sample displayed a protective action by reducing the number of reducible components that reach the anodic region and preventing the metal from

being oxidized by making it more passive. As such, when C2 demonstrated a decrease in i_{corr} from 2.54 x10^{-5} A/cm^2 to 4.44 x10^{-7} A/cm^2 with the corresponded changes of E_{corr}, the coatings are postulated to act as a mixed type inhibitor with a dominant inhibitive action in the anodic region. In regards to the efficiency calculation, which was made according to the values of polarization resistance, the C2 with 1 wt.% possessed the highest inhibition efficiency up to 91.2%, and it is in agreement with the findings in the previous characterization.

3.4. Scanning Electron Microscope (SEM)

The SEM analysis was conducted to investigate the condition of coatings after being subjected to a harsh medium for 15 days. Figure 5 shows the morphological surface under 1000x magnification for the coatings after the immersion process. Based on Figure 5(a), coating without MOE (C1) have multiple pores of the size 10 µm in diameter that signified an aggressive penetration of electrolytes into the coating matrix. With such a result, the performance of the coating can be expected to drop over time unless an additional protective mechanism by the pigments is initiated. Such a theory, however, can only be proved by prolonging the immersion period further. As for C3 and C4 illustrated in Figure 5(c) and Figure 5(d), both surfaces have tiny elongated cracks across the micrographs. These cracks may indicate a brittle property that is unfavorable as it will allow the electrolytes to pass through.

Additionally, there is also a clear formation of salt or NaCl crystals deposition on the surface of C4 that may cause a higher oxidation rate on the coating. As for C2, which was presented in Figure 5(b), the coating surface showed a small number of pores than other coatings. The finding aligned with other results that indicate C2 has superior properties in defending against aggressive ions. Nevertheless, with the presence of these pores, it is also an indication that the process of degradation has been initiated.

3.5. VOCs content study

The formulated coating with the best performance in the previous characterization was subjected to the VOCs content analysis using the standard ASTM. The coating was replicated with three replications to get the average measurement, and the result calculated was tabulated in Table 9. From the result, C2 with 1 wt.% of MOE showed a significantly low number of VOCs up to 198 g/L compared to the standard low VOCs limit for oil-based paint which was 380 g/L (U.S EPA). With low VOCs content, the paint can be deduced to pose a minimal detrimental effect on humans and the environment.

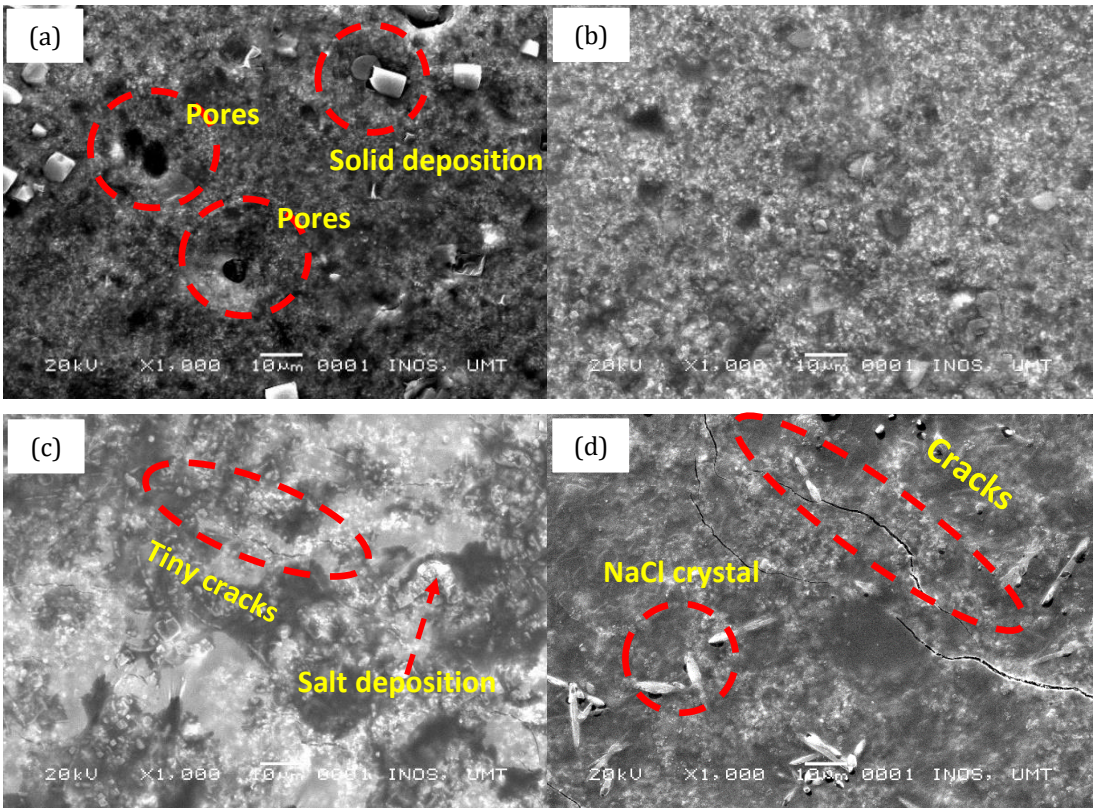

Fig. 5. SEM images of (a) C1, (b) C2, (C) C3 and (d) C4 after 15 days of immersion

Furthermore, this type of coating will also have less odor smell and dry quickly during the application stage. As mentioned previously, the importance of switching to low or no VOC paint can impart a significant change to the environment through the reduction of harmful ground-level ozone. However, most reputable suppliers of coatings nowadays tend to decrease the VOCs content even further as a means to promote the product and increase safety for the people. Hence, further research needs to be conducted to follow up on this trend while still ensuring the product's high efficiency.

Table 9. Measurement of total VOCs content for C2

Coating	Total Weight Fraction, TWF & Density (g/L)			
	Volatile		Non-volatile	
C2	TWF	Density	TWF	Density
	0.18	198.00	0.82	902.00

4. Conclusion

In conclusion, the optical analysis of the extract and formulated coatings revealed multiple presences of functional groups such as carboxylic acid with important heteroatoms that can boost the overall efficiency of the coating structure. This suggestion correlates with the result obtained in both EIS and polarization analysis where C2 with 1 wt.% of MOE exhibit the highest R_{ct} values of 12.32 x10^3 Ω and lowest corrosion rate of 4.64 x10^{-3} mm/year at the end of immersion test in comparison to the coating without the extract. Moreover, based on the recorded polarization resistance values, C2 displayed an outstanding inhibition efficiency of up to 92.1% compared with the bare stainless steel. Furthermore, through the morphological study, the surface of C2 after 15 days of immersion yielded a positive condition since no pores or cracks were detected. The outcome suggests that the barrier quality of the coating can slow down the penetration of the electrolyte effectively. Finally, the total VOCs investigation for C2 proved that the coating possessed low VOCs content of 198 g/L, which is suitable for marine application because of the minimal risk it posed to the environment.

Acknowledgments

This research was funded by the Ministry of Higher Education Malaysia through the Fundamental Research Grant Scheme (Award no. FRGS/1/2018/WAB09/UMT/02/2, Vot no. 59537). The authors also extend an appreciation for the support of the analytical analysis and testing center of Universiti Malaysia Terengganu.

Conflict of Interest

The author declares that there is no conflict of interest regarding the publication of this manuscript.

References

[1] Morin, J., Gandolfo, A., Temime-Roussel, B., Strekowski, R., Brochard, G., Bergé, V., Gligorovski, S. and Wortham, H., 2019. Application of a mineral binder to reduce VOC emissions from indoor photocatalytic paints. *Building and Environment, 156*, pp. 225-232.

[2] Sarwono, A., Man, Z., Idris, A., Nee, T.H., Muhammad, N., Khan, A.S. and Ullah, Z., 2018. Alkyd paint removal: Ionic liquid vs volatile organic compound (VOC). *Progress in Organic Coatings, 122*, pp. 79-87.

[3] Ismail, O.M.S. and Hameed, R.S.A., 2013. Environmental effects of volatile organic compounds on ozone layer. *Advances in Applied Science Research, 4*(1), pp. 264-268.

[4] Kasemy, Z.A., Kamel, G.M., Abdel-Rasoul, G.M. and Ismail, A.A., 2019. Environmental and health effects of benzene exposure among Egyptian taxi drivers. *Journal of environmental and public health, 2019*, pp. 1-6.

[5] Masih, A., Lall, A.S., Taneja, A. and Singhvi, R., 2016. Inhalation exposure and related health risks of BTEX in ambient air at different microenvironments of a terai zone in north India. *Atmospheric Environment, 147*, pp. 55-66.

[6] Chary, N.S. and Fernandez-Alba, A.R., 2012. Determination of volatile organic compounds in drinking and environmental waters. *Trends in Analytical Chemistry, 32*, pp. 60-75.

[7] Valdez, B., Ramirez, J., Eliezer, A., Schorr, M., Ramos, R. and Salinas, R., 2016. Corrosion assessment of infrastructure assets in coastal seas. *Journal of Marine Engineering & Technology, 15*(3), pp. 124-134.

[8] Pizzino, G., Irrera, N., Cucinotta, M., Pallio, G., Mannino, F., Arcoraci, V., Squadrito, F., Altavilla, D. and Bitto, A., 2017. Oxidative stress: harms and benefits for human health. *Oxidative Medicine and Cellular Longevity, 2017*, pp. 1-13.

[9] Mattioli, R., Mosca, L., Sánchez-Lamar, A., Tempera, I. and Hausmann, R., 2018. Natural bioactive compounds acting against oxidative stress in chronic, degenerative, and infectious diseases. *2018*, pp. 1-3.

[10] Puppel, K., Kapusta, A. and Kuczyńska, B., 2015. The etiology of oxidative stress in the various species of animals, a review. *Journal of the Science of Food and Agriculture, 95*(11), pp. 2179-2184.
[11] Allaoui, M., Rahim, O. and Sekhri, L., 2017. Electrochemical study on corrosion inhibition of iron in acidic medium by *Moringa oleifera* extract. *Oriental Journal of Chemistry, 33*(2), pp. 637-646.
[12] Gopalakrishnan, L., Doriya, K. and Kumar, D. S., 2016. *Moringa oleifera*: A review on nutritive importance and its medicinal application. *Food Science and Human Wellness, 5*(2), pp. 49-56.
[13] Odusote, J.K., Owalude, D., Olusegun, S. and Yahya, R., 2016. Inhibition efficiency of *Moringa oleifera* leaf extract on the corrosion of reinforced steel bar in HCl solution. *West Indian Journal of Engineering, 38*(2), pp. 64-70.
[14] Kamaruzzaman, W.M.I.W.M., Mohd-Fekeri, M.F., Shaifudin, M.S., Wan-Abdullah, W.R., Wan-Nik, W.M.N., Zulkifli, M.F.R. and Mohd-Ghazali, M.S., 2020. Enhancement of corrosion resistance and microbial protection analysis of a rosin coating with the incorporation of *Leucaena leucocephala*. *Coatings, 10*(9), pp. 1-20.
[15] Kamaruzzaman, W.M.I.W.M., Fekeri, M.F.M., Nasir, N.A.M., Hamidi, N.A.S.M., Baharom, M.Z., Adnan, A., Shaifudin, M.S., Abdullah, W.R.W., Wan Nik, W.M.N. and Suhailin, F.H., 2021. Anticorrosive and microbial inhibition performance of a coating loaded with *Andrographis paniculata* on stainless steel in seawater. *Molecules, 26*(11), pp. 1-18.
[16] Zulkifli, F., Yusof, M.S. M., Isa, M., Yabuki, A. and Nik, W.W., 2017. Henna leaves extract as a corrosion inhibitor in acrylic resin coating. *Progress in Organic Coatings, 105*, pp. 310-319.
[17] Savaloni, H., Agha-Taheri, E. and Abdi, F., 2016. On the corrosion resistance of AISI 316L-type stainless steel coated with manganese and annealed with flow of oxygen. *Journal of Theoretical and Applied Physics, 10*(2), pp. 149-156.
[18] Author (2003)*: ASTM Standard D2369-03*. West Conshohocken, PA, USA.
[19] Vergara-Jimenez, M., Almatrafi, M.M. and Fernandez, M.L., 2017. Bioactive components in *Moringa oleifera* leaves protect against chronic disease. *Antioxidants, 6*(4), pp. 1-13.
[20] Palou, R.M., Olivares-Xomelt, O. and Likhanova, N.V., (2014) 'Environmentally friendly corrosion inhibitors', in Aliofkhazraei, M. (ed.) *Developments in corrosion protection*. Rijeka, HR: IntechOpen, pp. 431-432.
[21] Calderón-Gutierrez, J.A. and Bedoya-Lora, F.E., 2014. Barrier property determination and lifetime prediction by electrochemical impedance spectroscopy of a high performance organic coating. *Dyna, 81*(183), pp. 97-106.
[22] Dong, Y. and Zhou, Q., 2014. Relationship between ion transport and the failure behavior of epoxy resin coatings. *Corrosion Science, 78*, pp. 22-28.
[23] Benedetti, A., Cirisano, F., Delucchi, M., Faimali, M. and Ferrari, M., 2016. Potentiodynamic study of Al–Mg alloy with superhydrophobic coating in photobiologically active/not active natural seawater. *Colloids and Surfaces B: Biointerfaces, 137*, pp. 167-175.
[24] Ikhmal, W.M.K.W.M., Fazira, M.M.F., Shaifudin, M.S., Amirah, N.M.N., Ghazali, M.S.M. and Rafizah, W.A.W., 2021. Assessment of corrosion efficiency and volatile organic compounds content for a green coating with novel additive of *Leucaena leucocephala*. *Journal of Sustainability Science and Management, 16*(4), pp. 37-52.